Journal of Clinical and Translational Hepatology **2026** vol. 14(3) | 301–316
DOI: 10.14218/JCTH.2025.00621

Original Article

LDLR$^+$ Monocytic Myeloid-derived Suppressor Cells Attenuate Allograft Rejection in Liver Transplantation

Xin Zhou[1,2#], Xinqiang Li[1,2#], Peng Jiang[1,2], Shipeng Li[3], Zhuoyu Jia[1,2], Xueteng Wang[1,2], Hailun Cai[4], Huan Liu[1,2], Ruidong Ding[1,2] and Jinzhen Cai[1,2,4*]

[1]Organ Transplantation Center, the Affiliated Hospital of Qingdao University, Qingdao, Shandong, China; [2]Institute of Organ Donation and Transplantation, Medical College of Qingdao University, Qingdao, Shandong, China; [3]Department of Hepato-pancreaticobiliary Surgery, Henan Provincial People's Hospital, Zhengzhou University, Zhengzhou, Henan, China; [4]Organ Transplant Center, Fujian Medical University Union Hospital, Fuzhou, Fujian, China

Received: November 20, 2025 | **Revised:** January 10, 2026 | **Accepted:** January 26, 2026 | **Published online:** February 27, 2026

Abstract

Background and Aims: Liver transplant rejection significantly affects patient prognosis. Myeloid-derived suppressor cells (MDSCs), known for their potent immunoregulatory functions, represent a promising target for managing liver transplant rejection. This study aimed to systematically characterize the diversity of MDSC subsets and their context-dependent functions, particularly within the context of transplant tolerance. ***Methods:*** We analyzed clinical and murine liver transplants using single-cell RNA sequencing, bulk RNA sequencing, flow cytometry, multiplex immunohistochemistry, and co-culture assays to phenotype MDSC subsets. ***Results:*** Single-cell RNA sequencing analysis of human and murine samples revealed MDSC involvement in transplant rejection. In mice, MDSC scores followed a normal distribution during the first week post-transplant and correlated with clinical flow cytometry data at one month. A distinct LDLR$^+$ monocytic MDSC (M-MDSC) subset was identified and confirmed through spatial mapping by multiplex immunohistochemistry. Flow cytometry demonstrated dynamic changes in LDLR$^+$ M-MDSCs across tissues (liver, spleen, peripheral blood, bone marrow, and lymph nodes), with a peak during acute rejection. Co-culture experiments showed that LDLR−/− M-MDSCs exhibited reduced Arg-1/iNOS expression and an impaired capacity to induce inhibitory receptors (TIGIT, PD1, CTLA-4) or suppress effector molecules (GZMB, IFN-γ, IL-2) in CD8$^+$ T cells. ***Conclusions:*** These findings highlight the critical role of MDSCs in liver transplant rejection. LDLR$^+$ M-MDSCs exhibited enhanced immunosuppressive properties, underscoring their potential clinical relevance in mitigating rejection and promoting immune tolerance.

Citation of this article: Zhou X, Li X, Jiang P, Li S, Jia Z, Wang X, *et al*. LDLR$^+$ Monocytic Myeloid-derived Suppressor Cells Attenuate Allograft Rejection in Liver Transplantation. J Clin Transl Hepatol 2026;14(3):301–316. doi: 10.14218/JCTH.2025.00621.

Keywords: Liver transplantation; Immune rejection; Immune tolerance; LDLR; Monocytic myeloid-derived suppressor cell; M-MDSC; Exhausted CD8$^+$ T cell.

[#]Contributed equally to this work.

[*]**Correspondence to:** Jinzhen Cai, Organ Transplantation Center, the Affiliated Hospital of Qingdao University, 59 Haier Road, Laoshan District, Qingdao, Shandong 266003, China. ORCID: https://orcid.org/0000-0001-5414-1050. Tel: +86-532-82915391. E-mail: caijinzhen@qdu.edu.cn.

Introduction

Liver transplantation (LT) represents a convergence of medical innovation and complex surgical expertise, offering a lifeline to patients with end-stage liver diseases. Despite substantial progress in immunosuppressive therapies that has markedly improved LT success rates and long-term outcomes, immune rejection remains a significant clinical challenge. Current immunosuppressive regimens, although indispensable, are associated with adverse effects such as infections, malignancies, hypertension, and nephrotoxicity.[1–3] Post-transplantation shifts in immune cell homeostasis and microenvironmental composition critically influence the development of immune rejection or tolerance, driven by intricate interactions among immune cell populations.[4–7] The ability to direct immune cell differentiation and modulate their functional properties holds considerable promise for precisely regulating immune responses. Such advancements may transform immunomodulation strategies and unlock new therapeutic opportunities. Therefore, investigating these dynamics and their underlying mechanisms is essential for improving clinical outcomes and deepening scientific understanding.

Myeloid-derived suppressor cells (MDSCs), a heterogeneous population of immature myeloid precursors, proliferate and accumulate in response to various pathological stimuli.[8] These cells are classified into monocytic MDSCs (M-MDSCs) and granulocytic MDSCs (G-MDSCs) subsets based on their myeloid lineage origins, and exhibit potent immunosuppressive properties, rendering them central to disease progression and immune regulation.[9] MDSCs suppress T cell function through multiple metabolic pathways, cytokine secretion, and signaling mechanisms in conditions such as cancer, autoimmune diseases, and infections.[10–12] Although the roles of MDSCs have been explored in several types of organ transplantation, there is a notable lack of research specifically focused on LT, particularly with respect to immune responses.[13,14] In our previous study, LDLR$^+$ MDSCs were found to expand in LT rejection tissues, as identified by single-cell RNA sequencing

(scRNA-seq), and were suggested to interact with T cells via the NECTIN2–TIGIT pathway to attenuate rejection.[15] Given their immunosuppressive potential, further investigation into the role of MDSCs in LT is warranted.

Therefore, by employing an integrated multi-omics strategy in conjunction with biological experiments, we aimed to delineate the heterogeneity and dynamic alterations of MDSCs within the context of liver transplant rejection. This comprehensive approach sought to advance the understanding of the immune microenvironment and critically assess the potential of MDSCs to promote immune tolerance.

Methods

Study subjects

This study included LT patients treated at the Organ Transplantation Center of Qingdao University Affiliated Hospital between November 2020 and November 2023. Post-transplant liver biopsies were obtained, incorporating data from a previous cohort.[16] All grafts were obtained from either donation after cardiac death or living donors, with approval from the hospital's Ethics Committee (IRB: QYFYWZLL29370).

Animals

Male C57BL/6J mice (8–10 weeks old, 23 ± 2 g; donors) and C3H/He mice (recipients) were purchased from Beijing Charles River and HFK Bioscience. LDL receptor–deficient (*LDLR*$^{-}$/$^{-}$) C57BL/6J mice (8 weeks old, 20 ± 2 g) were obtained from GemPharmatech. All animals were housed under specific pathogen–free conditions. Orthotopic liver transplantation (OLT) was performed under isoflurane anesthesia in accordance with established protocols and was approved by the Animal Welfare and Ethics Committee of Qingdao University (Approval No. 20221205C57C3H19220251205159).

Establishment of the mouse OLT model

The detailed surgical procedure[17] is provided in the Supplementary Method (Establishment of the Mouse Orthotopic Liver Transplantation Model).

Tissue dissection and cell suspension

Human liver biopsies, obtained immediately after transplantation, were preserved in a dedicated storage solution and processed using standard tissue dissociation techniques.[16] Samples were minced into 0.5 mm^3 fragments in RPMI-1640 medium (Invitrogen) supplemented with 1% penicillin–streptomycin, followed by enzymatic digestion at 37 °C for 30–45 min with constant agitation. The digestion cocktail included 0.05% trypsin (Invitrogen, Cat# 25200056), 0.4% collagenase IV (Invitrogen, Cat# 17104-019), 0.25% collagenase I (Sigma, Cat# C0130-1G), 0.13% collagenase II (BBI, Cat# A004174-0001), and 0.1% elastase (Worthington, Cat# LS002292). Resulting cell suspensions were sequentially filtered through 70 μm and 40 μm strainers (BD), centrifuged at 300 g for 10 min, treated with red blood cell lysis buffer (Thermo Fisher) on ice for 3 min, washed twice with PBS (Invitrogen), and resuspended in PBS containing 0.04% bovine serum albumin for downstream applications.

Mouse liver tissue was processed using the Liver Dissociation Kit (Miltenyi Biotec).[18] A dissociation mix was prepared in a gentleMACS™ C Tube by combining 4.7 mL DMEM with 200 μL Enzyme D, 100 μL Enzyme R, and 20 μL Enzyme A. Following a DMEM rinse, livers were transferred into the prepared C Tube, sealed, inverted, and processed using the gentleMACS Dissociator with program 37C_m_LIDK_1. The resulting cell suspension was filtered through a MACS® SmartStrainer (100 μm), rinsed with 5 mL DMEM containing stable glutamine, and centrifuged at 300 g for 10 min to remove the supernatant.

The procedures for preparing PBMCs from patients and mice, as well as the dissociation of multiple mouse tissues, are detailed in the Supplementary Method.[19–22]

Single-cell gene expression quantification and subcluster delineation

scRNA-seq data were processed using Seurat (v4.3.0)[23] following protocols established in our previous studies.[24–26] After importing the raw data, stringent quality control was performed to exclude cells with fewer than 501 detected genes or more than 25% mitochondrial transcripts. The remaining cells were normalized and scaled using Seurat's default parameters. Highly variable genes were identified using the FindVariableFeatures function and were employed for principal component analysis on the scaled data matrix. Dimensionality reduction and clustering were conducted using FindNeighbors (dims = 1:10) and FindClusters (resolution = 0.5). The transcriptional landscape was visualized using Uniform Manifold Approximation and Projection (hereinafter referred to as UMAP).

Cell type determination

Differentially expressed genes among clusters were identified using Seurat's FindMarkers and FindAllMarkers functions. Cell type annotation was guided by canonical marker genes from the CellMarker database (http://bio-bigdata.hrbmu.edu.cn/CellMarker/)[27] and corroborated with published studies. To improve classification accuracy, the SingleR package (v2.0.0)[28] was applied to match scRNA-seq profiles with reference datasets for robust cell identity assignment.

Functional enrichment analysis

Following cell type annotation, functional enrichment analysis of differentially expressed genes among clusters was conducted using Gene Ontology terms and Kyoto Encyclopedia of Genes and Genomes (KEGG) pathways. These analyses were carried out with the clusterProfiler package (v3.17.0)[28] in conjunction with the org.Hs.eg.db annotation database (v3.11.4). A *P*-value threshold of 0.05 was applied for both Gene Ontology and KEGG analyses. Enrichment results were visualized using bar plots or dot plots to summarize the key biological processes and pathways associated with each cell type.

MDSC scores

MDSC scores were calculated in Seurat using the AddModuleScore function and a set of marker genes associated with MDSCs.[29] Gene sets were curated based on published studies and publicly available datasets. For each cell, scores were derived from the aggregated expression levels of genes within the specified set, allowing assessment of expression patterns at the single-cell level.

Cell-cell communication analysis

Intercellular communication was examined using the CellChat package (v1.6.1),[30] which incorporates ligand–receptor interactions from the KEGG signaling pathway database and recent experimental findings. The analysis workflow comprised three main steps: identification of differentially expressed signaling genes, computation of ensemble average expression across cell types, and estimation of communication probabilities. This approach facilitated the mapping of

signaling networks and interaction patterns among distinct cell populations.

Bulk RNA sequencing analysis

To validate the findings, transcriptomic data were retrieved from the NCBI Gene Expression Omnibus. The GSE145780 dataset,[31] which comprises microarray-based liver transplant biopsy profiles from both rejection and non-rejection cases, was analyzed to evaluate gene expression differences associated with transplant outcomes.

Histological staining

Fresh liver tissue was fixed in 4% paraformaldehyde, embedded in paraffin, and sectioned at a thickness of 4 μm. Morphological evaluation was conducted using hematoxylin and eosin (H&E) staining.[32]

Immunohistochemistry (IHC) and multiplex immunohistochemistry (mIHC) staining analysis

For IHC, tissue sections were deparaffinized, rehydrated, and subjected to antigen retrieval, then blocked and incubated sequentially with primary and secondary antibodies.[33] Color development and counterstaining were then performed. For mIHC, prepared slides underwent microwave heating, blocking, and antibody incubation, with signal amplification. These steps, microwave heating, blocking, and antibody incubation, were repeated as necessary, followed by DAPI counterstaining and mounting.[34] Stained slides were scanned using a Pannoramic MIDI scanner (3DHISTECH, Hungary), and images were analyzed with the HALO 2.0 Area Quantification algorithm (Indica Labs, Corrales, NM) at Nanjing Freethinking Biotechnology Co., Ltd. (China).

Flow cytometry

For flow cytometric analysis, cells were stained using multiple panels of fluorochrome-conjugated antibodies, including anti-CD45, anti-HLA-DR, anti-CD11b, anti-CD33, anti-CD14, anti-CD15, anti-Ly6C, anti-Ly6G, anti-LDLR, anti-NECTIN2, anti-PDL1, anti-Arg-1, anti-iNOS, anti-CD8A, anti-TIGIT, anti-CTLA-4, anti-PD1, anti-GZMB, anti-IFN-γ, and anti-IL-2. All antibodies were obtained from BioLegend and Invitrogen.

For cell surface staining, cells were adjusted to 5–10 × 10^6/mL in 100 μL of 1× PBS containing 5% bovine serum albumin and blocked in the dark for 15 min. Primary antibodies were then added and incubated for 15–20 min, followed by two washes and resuspension for flow cytometric analysis.[35]

For intracellular staining, cells were first blocked and incubated with primary surface antibodies as described above, then washed and fixed with 100 μL of fixation buffer (Invitrogen) for 30 min. Following permeabilization (Invitrogen), cells were incubated with primary intracellular antibodies for 20 min, washed twice, and resuspended for analysis.[35] Samples were acquired using a flow cytometer (CytoFLEX S, USA) and analyzed with FlowJo software (v10.8.1) to quantify cell populations based on fluorescence intensity and antibody binding.

Co-culture experiment

Bone marrow cells were harvested from the tibias and femurs of wild-type and Ldlr$^{-/-}$ C57BL/6J mice by flushing with 1× PBS. Red blood cells were lysed using ACK lysis buffer, and the remaining cells were plated in 25 cm^2 culture flasks (Corning, USA). For M-MDSC induction, bone marrow cells (1 × 10^6/mL) were cultured in DMEM (HyCyte, China) supplemented with 40 ng/mL GM-CSF and IL-6 at 37 °C in 5% CO_2 for four days.[36] M-MDSCs were then isolated using magnetic microbeads (Miltenyi Biotec).[37]

Single-cell suspensions prepared from lymph nodes were used to isolate CD8$^+$ T cells with CD8a microbeads (Miltenyi Biotec).[38] For co-culture assays, 1 × 10^6 CD8$^+$ T cells were cultured with M-MDSCs in 2 mL RPMI 1640 medium (HyCyte, China) in 6-well round-bottom plates for three days, followed by flow cytometric analysis.

Statistical analysis

Statistical analyses and data visualization were performed using R (v4.3.0) and GraphPad Prism (v8.0.2). Data are presented as mean ± standard error of the mean. Differences between two groups were assessed using an unpaired Student's t-test, whereas comparisons among multiple groups were evaluated using the Kruskal–Wallis H test. Statistical significance is denoted as *P < 0.05, ** P < 0.01, and *** P < 0.001.

Results

scRNA-seq analysis highlights myeloid cells in patients after LT

As an initial step, the myeloid immune cell repertoire of patients following LT (post-LT) was characterized using scRNA-seq profiling. Unsupervised clustering identified 11 distinct clusters among 18,148 myeloid cells. Canonical marker genes (Supplementary Table 1) were analyzed to annotate specific cell types (Fig. 1A), including dendritic cells, Kupffer cells, macrophages, and MDSCs (Fig. 1B). Tissue distribution analysis revealed a predominance of macrophages in liver samples (20.3%, 16.2%, 52%, and 11.5%), whereas peripheral blood samples were overwhelmingly enriched in macrophages (4.0%, 1.1%, 78.2%, and 16.8%) (Fig. 1C). Macrophages (clusters C0, C1, C3, C4, and C7), characterized by the expression of *S100A9*, *CD68*, and *FCN1* (Fig. 1D), were significantly enriched in rejection tissues (Fig. 1E), indicating a potential key role in immune regulation following LT. In contrast, dendritic cells (C5, C8, C10), defined by the expression of *CD1C*, *CLEC10A*, *FCER1A*, and *IRF8*, and Kupffer cells (C6, C9) were reduced in rejection samples. MDSCs (C2), identified by *S100A8*, *S100A9*, *FCN1*, and *VCAN*, were predominantly liver-derived and showed elevated abundance in rejection tissues.

IHC staining of liver biopsies from patients with mild and severe acute rejection revealed pronounced immune cell infiltration in the portal areas (Supplementary Fig. 1A). CD4$^+$ and CD8$^+$ T cells, along with CD68$^+$ macrophages, were markedly increased, suggesting their involvement in the immunopathology of acute rejection.

scRNA-seq analysis unveils functionally distinct subsets of MDSCs

The aforementioned cells represent key components of the immune response following LT. However, the present study focuses specifically on MDSCs. Further analysis revealed three distinct MDSC subsets: C0-LIPA$^+$ MDSC, C1-LDLR$^+$ MDSC, and C2-S100P$^+$ MDSC (Fig. 2A). Violin plots demonstrated that all subsets expressed characteristic MDSC markers, including *S100A8* and *S100A9* (Fig. 2B). Notably, the C1-LDLR$^+$ MDSC subset exhibited significantly higher expression levels of these markers. Given the established association between *S100A8* and *S100A9* and MDSC proliferation, these findings suggest that C1-LDLR$^+$ MDSCs may possess enhanced immunosuppressive capacity compared with the other subsets.

All clusters exhibited high *CD14* expression and relatively

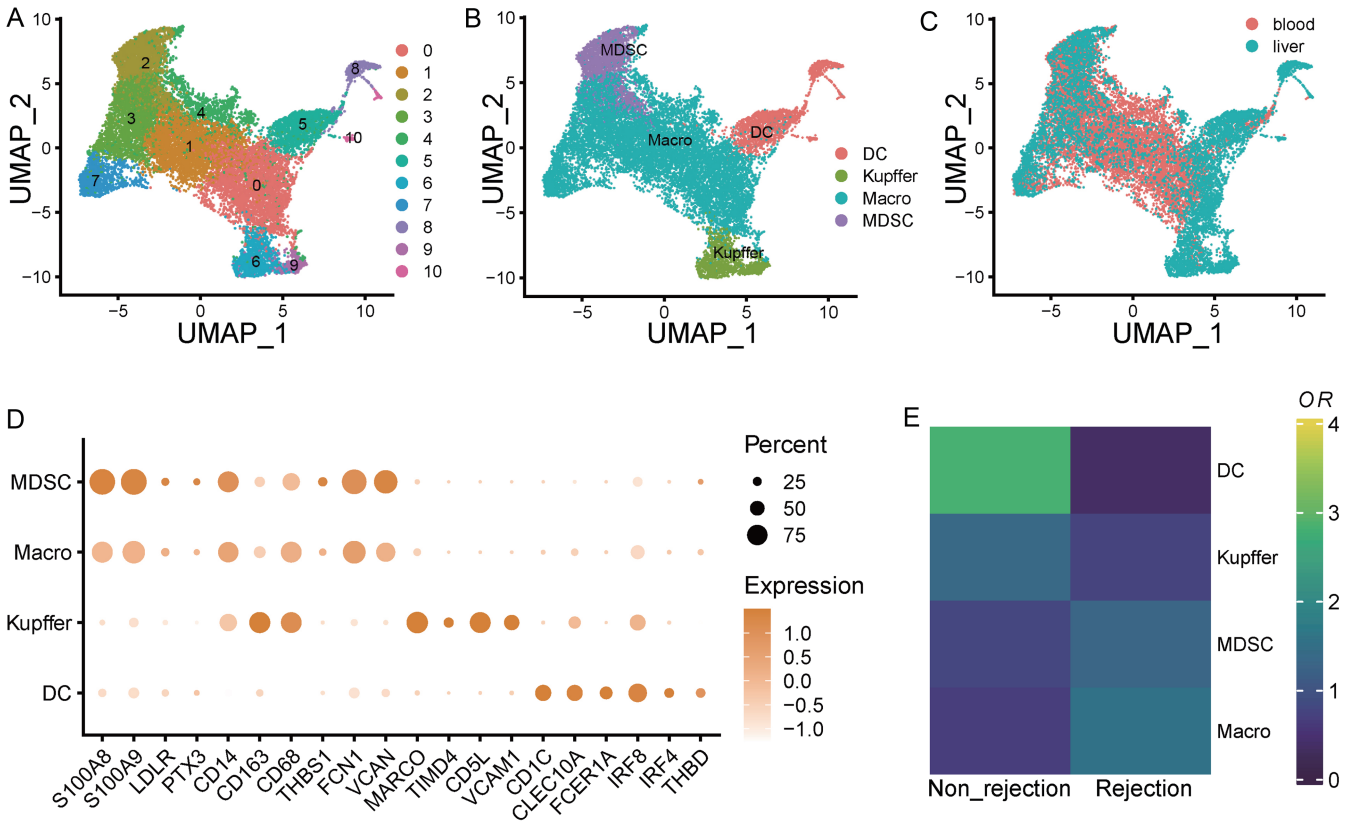

Fig. 1. scRNA-seq analysis of humans after liver transplantation. (A) UMAP of myeloid cells divided into 11 clusters. (B) UMAP plot colored by tissue source (liver and peripheral blood). (C) UMAP plot colored by cell type. (D) Dot plot showing the representative gene expression of clustered cells. (E) Heatmap showing the OR of cell clusters for non-rejection (left) and rejection patients (right). scRNA-seq, single-cell RNA sequencing; UMAP, uniform manifold approximation and projection; OR, odds ratio.

low *CD15* expression. Immunohistochemical analysis further confirmed that MDSCs in liver tissues with varying degrees of rejection predominantly displayed monocytic characteristics (Supplementary Fig. 2).

A total of 227 differentially expressed genes were identified across the three clusters (Supplementary Table 2). The C0-LIPA⁺ MDSC subset expressed genes associated with lysosomal function, including *LIPA* and *PLD3*. Compared with the other subsets, C0-LIPA⁺ MDSCs showed greater enrichment for genes involved in mitochondrial function (such as *MT-ND1*, *MT-ATP6*, *MT-CO1*, and *MT-CO3*). These genes encode key enzymes that are integral components of the mitochondrial electron transport chain, which plays a critical role in cellular respiration and energy production. The C1-LDLR⁺ MDSC subset exhibited a distinct metabolic profile characterized by elevated expression of lipid metabolism markers (*LDLR*, *PLIN2*, *OLR1*) and glucose metabolism–related genes (*GK*, *TYMP*). This profile suggests metabolic reprogramming potentially linked to immune regulation in the context of metabolic disorders. The C2-S100P⁺ MDSC subset preferentially expressed genes involved in cellular signaling, including *TLR4*, *PTPRE*, and *TRIB1*, suggesting a role in modulating immune regulatory networks.

Distinct differences in the expression of immune function–related genes were observed across the three MDSC subsets. The C0-LIPA⁺ MDSC subset favored antigen presentation and immune cell recognition, with significant expression of genes encoding MHC class II molecules, including *HLA-DPA1*, *HLA-DQA1*, and *HLA-DRA*. These genes are critical in antigen-presenting cells for initiating antigen-specific immune responses. Functional enrichment analysis revealed significant involvement in regulating lymphocyte proliferation and the negative regulation of leukocyte cell–cell adhesion (Fig. 2E and Supplementary Table 3). The C1-LDLR⁺ MDSC subset expressed genes directly associated with inflammatory response regulation, including chemokines (*CXCL2*, *CXCL3*, *CXCL8*), interleukin-related genes (*IL1β* and *IL6R*), and *NLRP3*, a key component of the inflammasome complex. These genes are essential for immune cell recruitment, activation, and signal transduction. Functional enrichment analysis highlighted roles in modulating acute inflammatory responses and promoting immune tolerance, with potential implications for the regulation of liver transplant rejection. The C2-S100P⁺ MDSC subset exhibited elevated expression of genes associated with antiviral defense, such as *IFIT1*, *IFITM3*, and *RSAD2*, suggesting a specialized role in antiviral immunity. Functional enrichment further supported involvement in the negative regulation of viral processes and modulation of innate immune responses.

We further mapped the intercellular communication network. The dot plot illustrated predicted ligand–receptor interactions among MDSCs, CD8⁺ T cells, and regulatory T cells (Tregs) (Fig. 2C and D). The analysis suggests potential interactions mediated by HLA-E/KLRK1 and LGALS9/CD45 ligand–receptor pairs (Supplementary Table 4).

LDLR⁺ MDSCs participate in rejection after LT

To validate the scRNA-seq findings, flow cytometry was per-

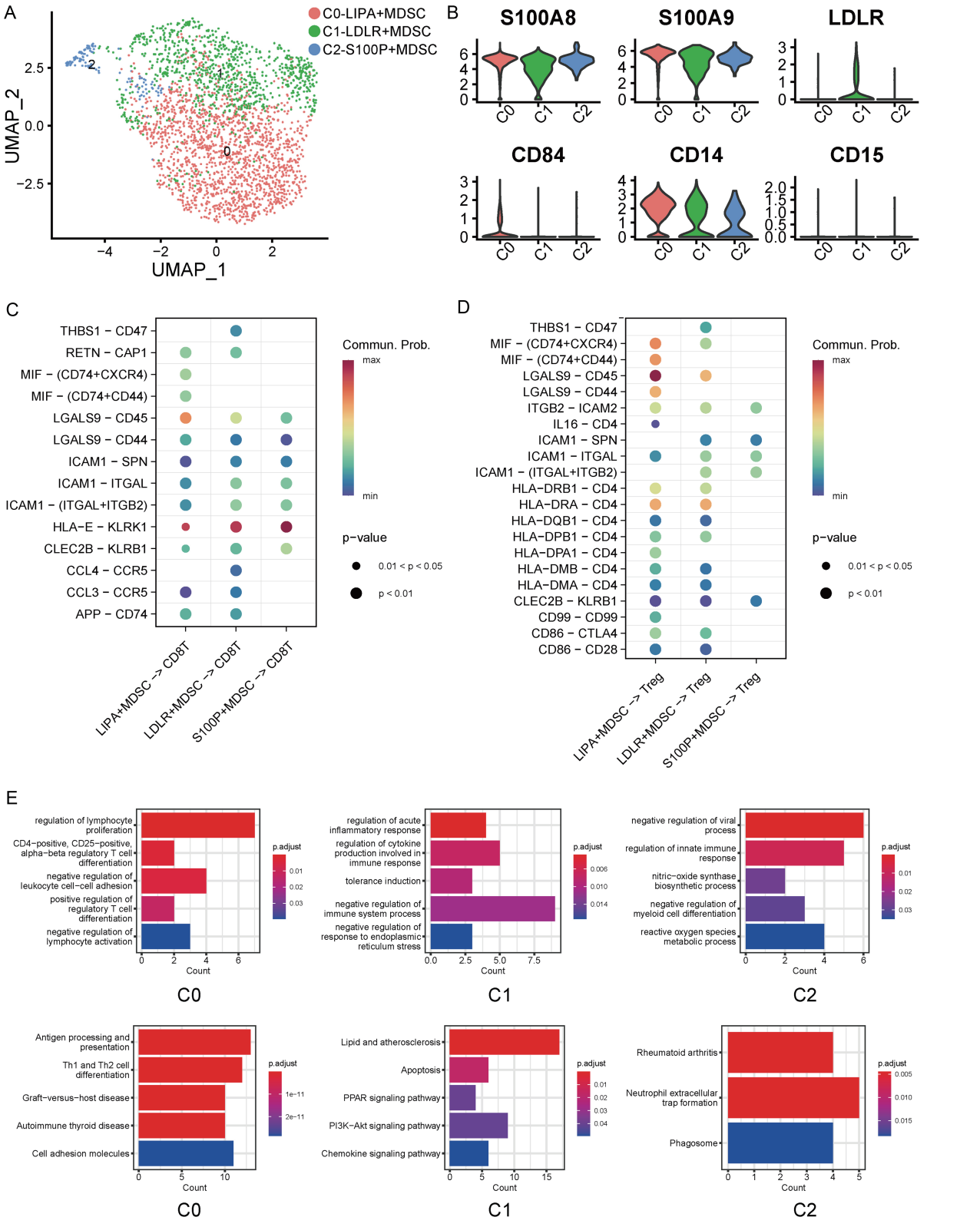

Fig. 2. Identification of MDSC subsets in human transplanted liver and peripheral blood. (A) UMAP plot for re-clustering of MDSCs. (B) Violin plot illustrating differentially expressed genes in MDSCs. (C) Dot plot showing cellular communication between MDSCs and CD8^{+} T cells. (D) Dot plot showing cellular communication between MDSCs and Tregs. (E) Bar plots illustrating Gene Ontology and KEGG pathway enrichment analyses among the three clusters. MDSCs, myeloid-derived suppressor cells; UMAP, uniform manifold approximation and projection; Tregs, regulatory T cells; KEGG, Kyoto Encyclopedia of Genes and Genomes.

formed on peripheral blood samples collected from post-LT patients (Fig. 3A). The gating strategy for MDSCs is provided in Supplementary Figure 3A. Following LT, the proportion of MDSCs among immune cells increased rapidly, remained elevated during the acute phase (up to seven days), and subsequently declined to preoperative levels. Within the MDSC compartment, the proportion of M-MDSCs increased progressively throughout the acute phase, peaking on POD7, and then gradually decreased. Moreover, similar temporal trends were observed in the proportion of M-MDSCs relative to the total immune cell population.

In the bulk RNA sequencing analysis (Fig. 3B), a significant elevation in the expression of the myeloid cell marker *CD11b* was observed in rejection samples. Markers associated with MDSCs, including *S100A8* and *S100A9*, were also significantly upregulated in the rejection group. Although *LDLR* expression was increased in rejection samples, the difference did not reach statistical significance. Additionally, a significant upregulation of immune checkpoint molecules—*NECTIN2*, *PDL1*, and *TIGIT*—was observed, consistent with our previous findings. mIHC performed on transplanted liver samples exhibiting varying degrees of rejection (mild and severe acute rejection, as well as chronic rejection) confirmed the presence of LDLR$^+$ M-MDSCs and LDLR$^+$ G-MDSCs (Fig. 3C and Supplementary Fig. 3B).

scRNA-seq analysis identifies specific subsets of MDSCs within mouse OLT models

To further substantiate the role of LDLR$^+$ MDSCs in graft rejection, scRNA-seq analysis was performed using a mouse OLT model (C57BL/6J to C57BL/6J) across seven time points: preoperative LT (pre-LT), 3 h post-LT, 6 h post-LT, 12 h post-LT, POD3, POD5, and POD7.[39] This dataset generated a comprehensive myeloid cell atlas comprising 14,372 cells. The analysis identified 14 distinct clusters, visualized using UMAP plots that illustrated their distribution across the dynamic time course (Fig. 4A, B, and Supplementary Table 5). Among them, nine macrophage clusters, three monocyte clusters, and two MDSC clusters were identified.

Consistent with the human scRNA-seq findings, cluster C2 was annotated as LDLR$^+$ MDSC. This subset exhibited elevated expression of lipid metabolism–related genes, including *LDLR* and *OLR1*. Source analysis of C2-LDLR$^+$ MDSCs revealed that the majority of cells originated from the 12 h post-LT time point (59%). Within the datasets corresponding to the first 12 h after transplantation, *NFKBIA* expression levels were notably elevated (Fig. 4C). Longitudinal gene expression analysis demonstrated a significant increase in *ARG1* expression from POD3 to POD7, whereas *NOS2* expression remained relatively unchanged. Using the MDSC gene signature, gene-scoring analysis was performed across the identified clusters (Fig. 4D). The analysis revealed a substantial increase in MDSC-associated scores within the first 24 h following LT, with peaks at 3, 6, and 12 h post-LT. Scores subsequently declined by POD3 and POD7, indicating a temporal pattern of MDSC activation.

To simulate immune-state transitions following transplantation, four mouse OLT rejection models (C57BL/6J to C3H/He) were established. Liver tissues were collected at sequential time points—one, two, three, and four weeks post-LT—and analyzed using H&E staining, IHC, mIHC, and flow cytometry to evaluate tissue damage and immune cell infiltration during the transition from acute rejection to immune tolerance (Fig. 4E). H&E staining revealed pronounced immune cell infiltration in the portal areas, accompanied by pathological features such as hepatocyte necrosis, bile duct injury, and sinusoidal congestion, which were particularly prominent compared with normal liver tissue (Fig. 4F and Supplementary Fig. 4C). Immune infiltration peaked at two and three weeks post-LT, with a marked reduction by four weeks. IHC staining for CD3, CD4, CD8, and FOXP3 confirmed the presence of the corresponding lymphocyte subsets (Fig. 4F and Supplementary Fig. 4A).

Specifically, CD8$^+$ T cell infiltration peaked at two weeks post-LT, as illustrated in the bar graph (Supplementary Fig. 4B). Overall, lymphocyte infiltration increased sharply at one and two weeks post-LT and then gradually declined at three and four weeks post-LT.

Dynamic, multi-tissue changes of LDLR$^+$ M-MDSCs in mouse OLT models

To comprehensively assess the dynamics of MDSCs in mouse OLT models (C57BL/6J to C3H/He), tissues including liver, spleen, peripheral blood, lymph nodes, and bone marrow were collected across the post-LT timeline (one, two, three, and four weeks post-LT) for mIHC and flow cytometry analysis, with quantification expressed as n/CD11b%. mIHC revealed variable infiltration of LDLR$^+$ M-MDSCs in the portal areas of transplanted livers, peaking at one week post-LT (Fig. 5A). Flow cytometry, using gating strategies to distinguish G-MDSCs (CD11b$^+$Ly6C^{low}Ly6G$^+$) and M-MDSCs (CD11b$^+$Ly6C^{high}Ly6G$^-$) (Supplementary Fig. 5), revealed distinct temporal distributions across different tissues (Fig. 5B).

The results demonstrated that the proportions of various cell populations in the bone marrow increased at one week post-LT. Following this initial rise, the proportions of myeloid cells (CD11b/Alive) and G-MDSCs stabilized, whereas the proportions of M-MDSCs and their subsets gradually declined over time. A similar trend was observed in the liver, where myeloid cell proportions increased at one week post-LT, followed by a fluctuating decrease; however, levels at four weeks post-LT remained elevated compared with pre-LT values. The proportion of G-MDSCs showed an upward trend throughout the observation period. Notably, M-MDSCs and their subsets displayed a sharp increase at one week post-LT, representing the most pronounced change among all tissues, followed by a gradual decline.

In the spleen, a distinct pattern was observed: the proportions of myeloid cells, G-MDSCs, and M-MDSCs gradually increased over the first three weeks post-LT and then declined. In contrast, the proportions of M-MDSC subsets decreased modestly within the first two weeks post-LT and then gradually returned to pre-LT levels. In peripheral blood, the proportion of LDLR$^+$ M-MDSCs increased slowly, peaking at two weeks post-LT, and then declined, while the proportions of other cell types fluctuated throughout the observation period. In the lymph nodes, the proportion of myeloid cells remained relatively stable, and the proportion of G-MDSCs was nearly undetectable. Meanwhile, the proportions of M-MDSCs and their subsets demonstrated variable, fluctuating patterns over time.

Detailed statistical analyses of M-MDSCs and their subsets (n/Alive%) across different tissues revealed significant differences, particularly at one week post-LT (Fig. 6 and Supplementary Fig. 6). In both the liver and bone marrow, the previously described trend—an initial increase followed by a gradual decrease—was consistently validated. By three weeks post-LT, increased variability in the spleen and peripheral blood made it challenging to achieve statistical significance, although the overall trends in M-MDSC subsets remained evident. In the lymph nodes, aside from the statistically significant increase observed at one week post-LT, the

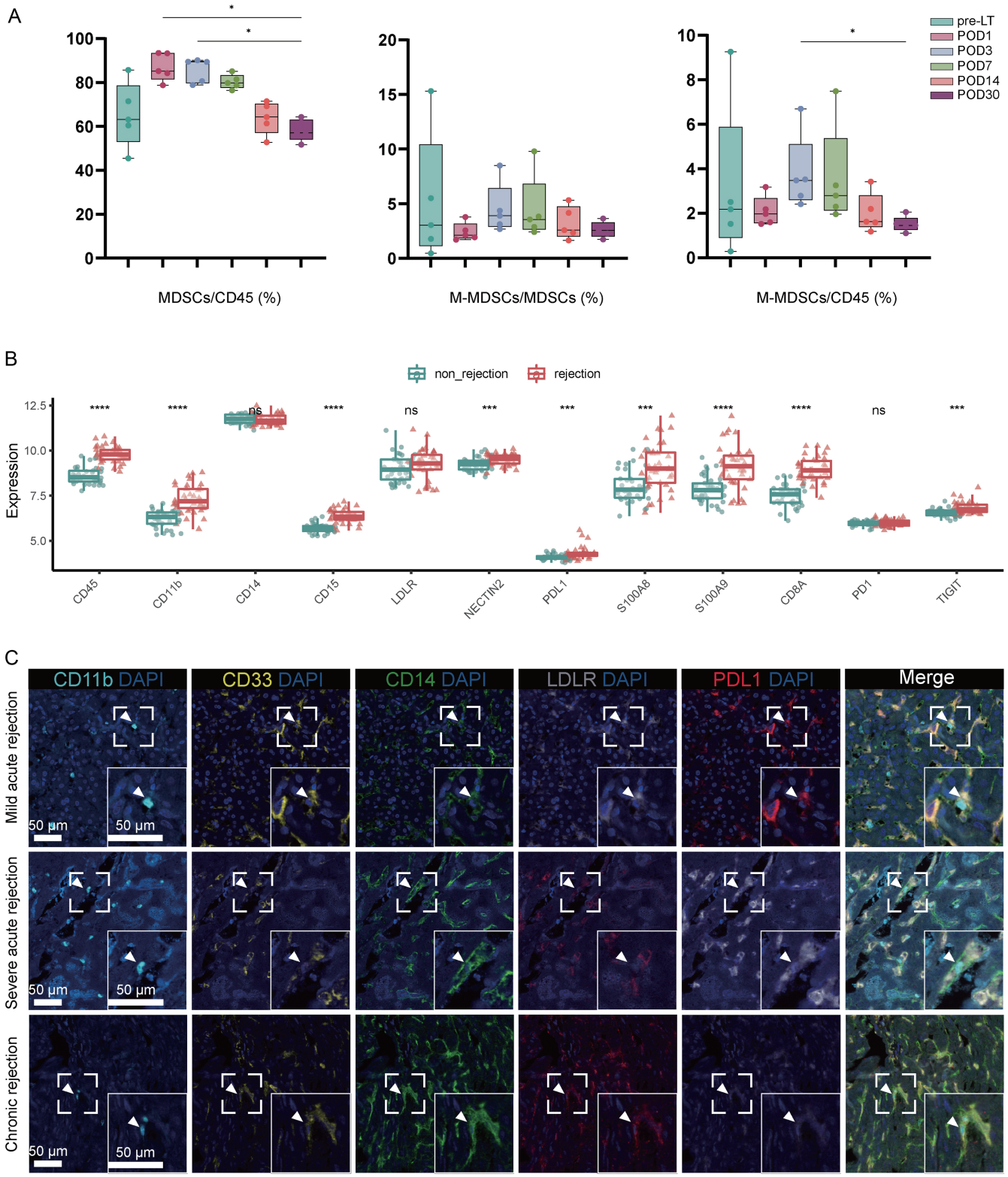

Fig. 3. Identification of marker expression of MDSCs during rejection. (A) Flow cytometry showing dynamic changes in MDSCs and M-MDSCs in peripheral blood post-LT. (B) Gene expression of MDSC-related markers between non-rejection and rejection samples using bulk RNA sequencing. (C) mIHC of DAPI (blue), CD11b (cyan), CD33 (yellow), CD14 (green), LDLR (gray), and PDL1 (red) in transplanted livers with different severities of rejection. White arrows indicate cells co-expressing CD11b, CD33, CD14, LDLR, and PDL1. Whole/insert image scale bar, 50 μm. *p < 0.05. MDSCs, myeloid-derived suppressor cells; M-MDSCs, monocytic myeloid-derived suppressor cells; LT, liver transplantation; mIHC, multiplex immunohistochemistry.

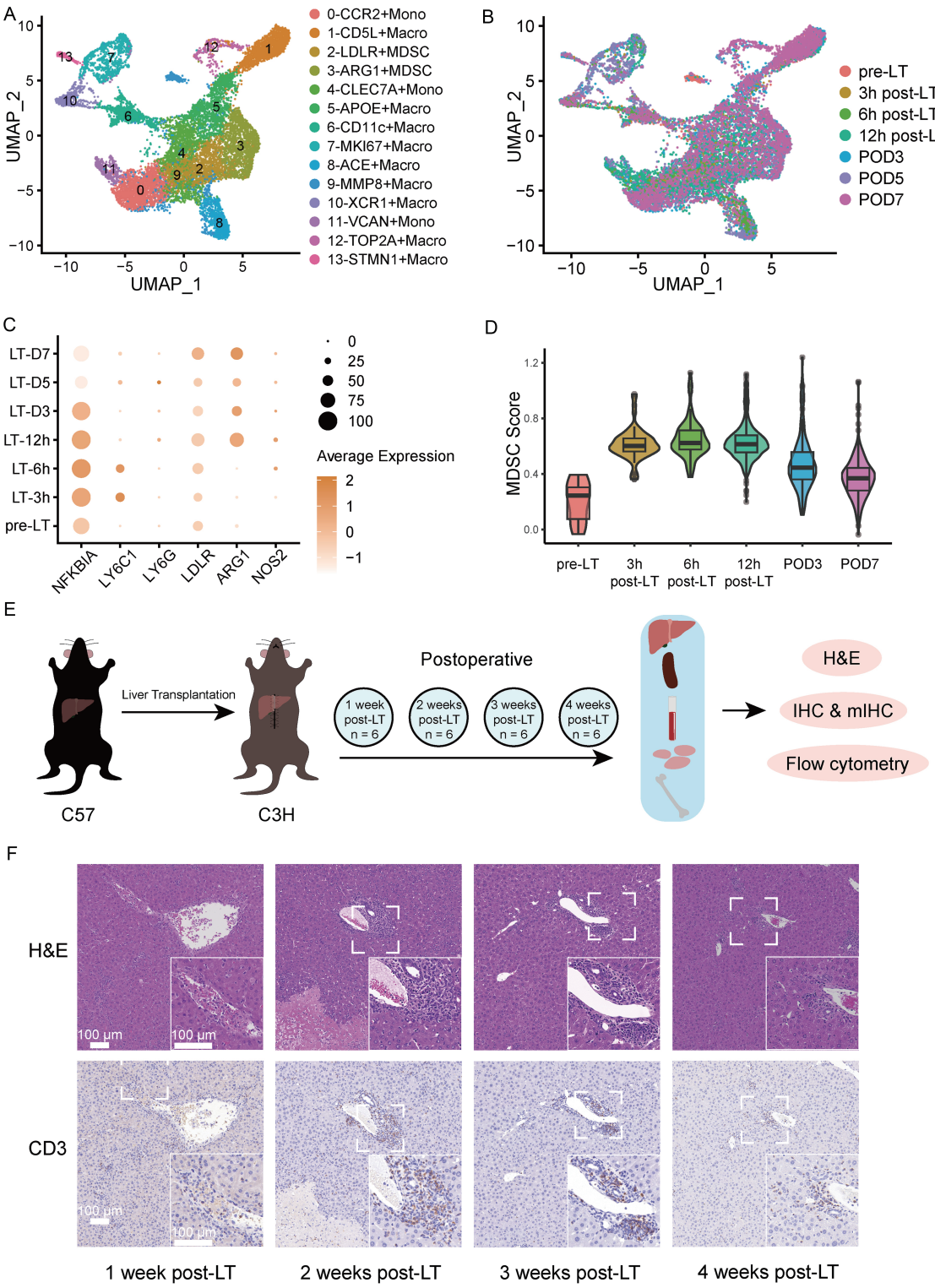

Fig. 4. Identification of myeloid cell subsets at multiple time points after transplantation. (A) UMAP plot of myeloid cells divided into 14 identified clusters. (B) UMAP plot colored by chronological time points post-LT. (C) Dot plot showing gene expression in C2-LDLR-MDSCs across chronological time points post-LT. (D) Violin plot illustrating MDSC scores across chronological time points post-LT. (E) Establishment of mouse OLT models with defined time intervals for sample collection (liver, spleen, peripheral blood, bone marrow, lymph nodes). Livers were used for IHC and mIHC, and livers, spleen, peripheral blood, lymph nodes, and bone marrow were used for flow cytometry. (F) H&E staining and IHC of CD3 in transplanted livers obtained from mouse OLT models. Whole/insert image scale bar, 100 μm. UMAP, uniform manifold approximation and projection; LT, liver transplantation; MDSCs, myeloid-derived suppressor cells; OLT, orthotopic liver transplantation; IHC, immunohistochemistry; mIHC, multiplex immunohistochemistry; H&E, hematoxylin and eosin.

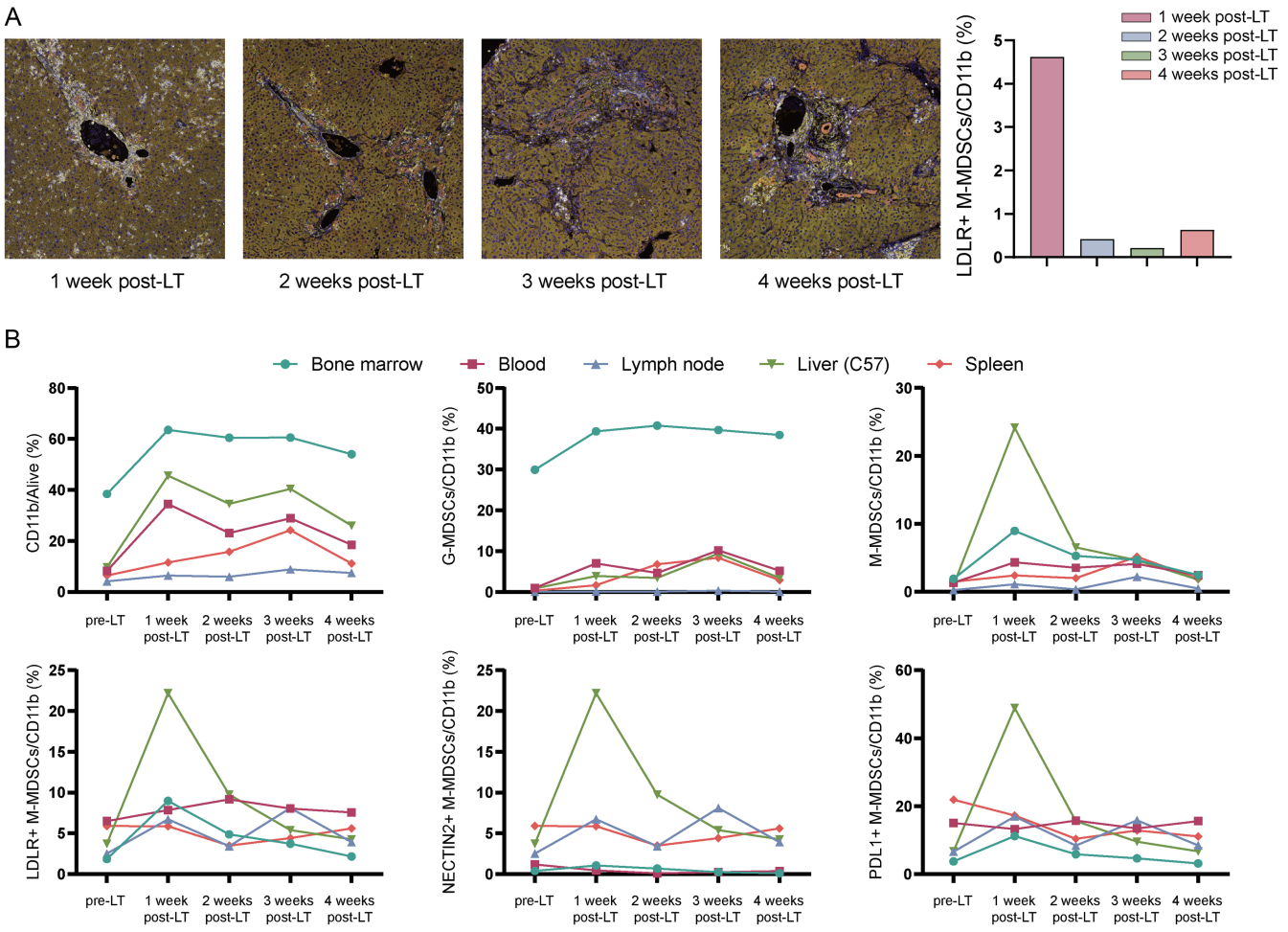

Fig. 5. Flow cytometry shows temporal variation in M-MDSCs across different tissues. (A) mIHC of DAPI (blue), CD11b (yellow), Ly6C (white), and LDLR (magenta) in transplanted livers. Whole/insert image scale bar, 100 μm. The bar graph represents quantification of CD11b$^+$ Ly6C$^+$ LDLR$^+$ cells (LDLR$^+$ M-MDSCs). (B) Line chart illustrating dynamic changes in cell proportions across distinct tissue types. *p < 0.05. **p < 0.01. ***p < 0.001. M-MDSCs, monocytic myeloid-derived suppressor cells; mIHC, multiplex immunohistochemistry.

proportions of M-MDSCs and their subsets remained consistently low across the remaining time points.

LDLR$^+$ M-MDSCs induced exhaustion of CD8$^+$ T cells

mIHC was employed to map the spatial distribution of LDLR$^+$ M-MDSCs and TIGIT$^+$ CD8$^+$ T cells across the post-LT timeline (Supplementary Fig. 7A). Proximity analysis using Ripley's K-function revealed a significantly enhanced spatial clustering between these cell populations at four weeks post-LT (Fig. 7A). Co-culture experiments were conducted to verify whether LDLR$^+$ M-MDSCs possessed stronger immunosuppressive capabilities. Microbeads were used to isolate M-MDSCs and LDLR$^{-/-}$ M-MDSCs from bone marrow cells induced *in vitro*, which were then co-cultured with CD8$^+$ T cells (Fig. 7B). Supplementary Figure 7B shows the flow cytometric analysis of M-MDSCs purified by microbeads (CD11b$^+$Ly6C$^+$). Flow cytometry assessed changes in exhaustion markers (TIGIT, PD1, and CTLA-4), functional markers of CD8$^+$ T cells (GZMB, IFN-γ, and IL-2), and functional markers of MDSCs (Arg-1 and iNOS). The gating strategy is shown in Supplementary Figures 7C–E. The results demonstrated that wild-type M-MDSCs significantly increased the levels of exhaustion markers and decreased the expression of functional markers, whereas the capacity of LDLR$^{-/-}$ M-MDSCs was comparatively weaker (Figs. 7C and 8C).

Following microbead-based sorting of M-MDSCs, flow cytometry was immediately performed to assess the expression of functional markers. The analysis revealed that wild-type M-MDSCs exhibited significantly higher expression of iNOS compared with LDLR$^{-/-}$ M-MDSCs (Fig. 8A). Further examination of functional markers in co-cultured M-MDSCs showed elevated expression levels of both Arg-1 and iNOS, exceeding those observed in LDLR$^{-/-}$ M-MDSCs (Fig. 8B). Notably, LDLR$^{-/-}$ M-MDSCs did not show a significant change in iNOS expression relative to wild-type M-MDSCs.

Discussion

Achieving immune tolerance following organ transplantation is essential, particularly for patients at high risk of rejection or with a history of prior rejection episodes. Identifying safe and effective target cells or therapeutic agents remains a critical priority. MDSCs have emerged as key mediators due to their potent immunosuppressive functions, which operate through multiple mechanisms.[40–42] In oncology, chemokines recruit MDSCs to tumor sites, where they contribute to im-

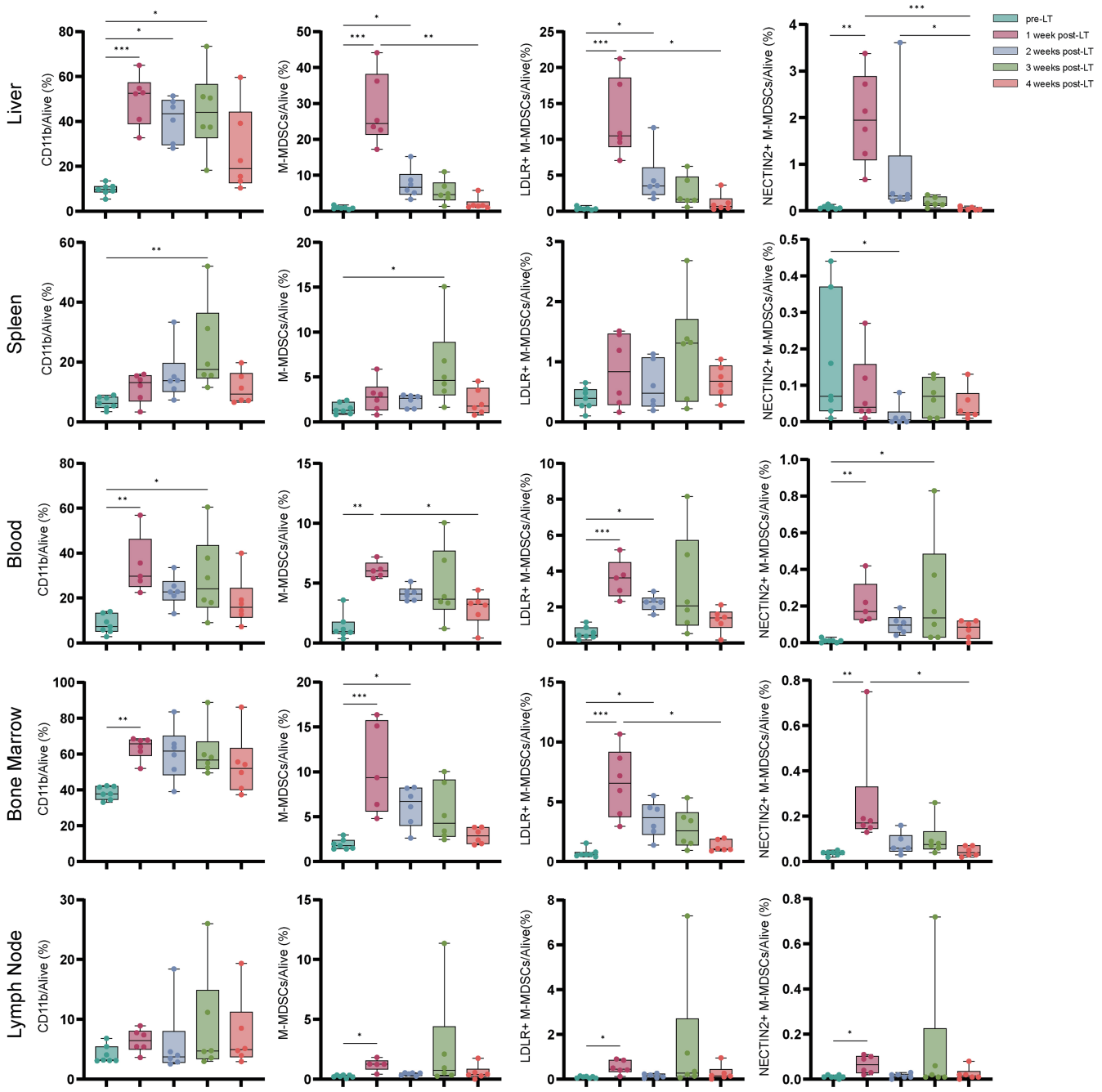

Fig. 6. Detailed analysis of M-MDSCs in different tissues. Box plots depicting statistical analyses of cell proportion changes over time within specific tissues. *p < 0.05. **p < 0.01. ***p < 0.001. M-MDSCs, monocytic myeloid-derived suppressor cells.

mune dysfunction, resistance to immunotherapy, and tumor progression.[43–46] In the context of infectious diseases, MDSCs suppress T cell activity primarily by increasing ROS production.[47,48] Collectively, these findings highlight the role of inflammatory conditions in driving MDSC activation and expansion, positioning them as central components of the pathological immune microenvironment.[49–51] In this study, we employed multi-omics approaches to conduct a comprehensive bioinformatic analysis of MDSCs in the context of liver transplant rejection. We elucidated their role in the rejection process, characterized the post-transplant dynamics of MDSC subsets, and validated their functional mechanisms through *in vitro* experiments.

Analysis of human scRNA-seq data revealed that MDSCs exhibit low heterogeneity and are predominantly liver-derived, likely reflecting the inflammatory microenvironment that promotes their recruitment and accumulation during transplant rejection. This recruitment process parallels the infiltration of MDSCs into the tumor microenvironment, which occurs through diverse chemokine-mediated pathways.[52,53]

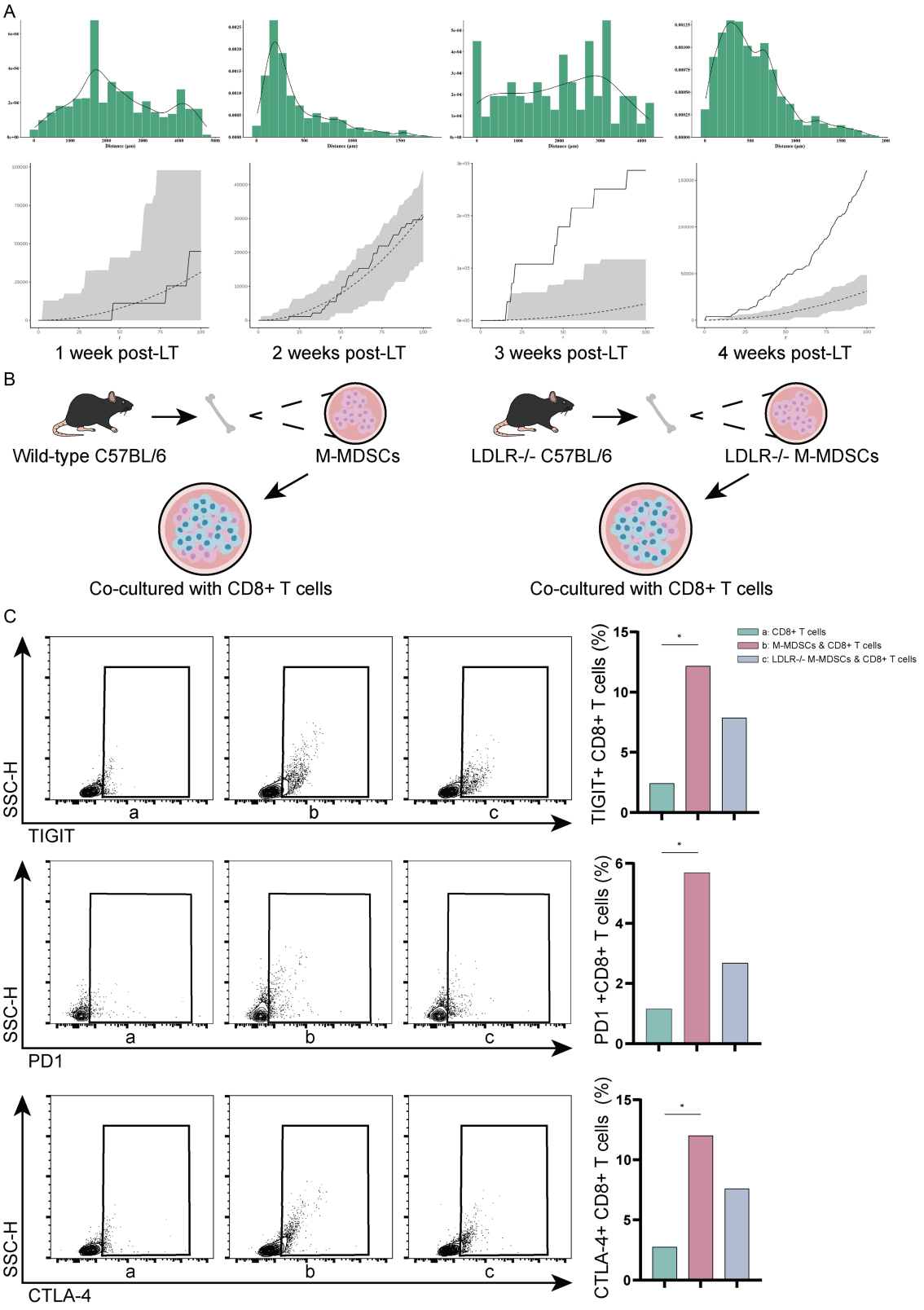

Fig. 7. Interactions between LDLR$^+$ M-MDSCs and CD8$^+$ T cells. (A) Proximity analysis and Ripley's K-function calculations for LDLR$^+$ M-MDSCs and TIGIT$^+$ CD8$^+$ T cells. Solid lines represent observed K(r), while dashed lines indicate theoretical K(r). (B) Diagram of the co-culture experiment. (C) Flow cytometry analysis of exhaustion markers in CD8$^+$ T cells co-cultured with M-MDSCs and LDLR−/− M-MDSCs. *p < 0.05. **p < 0.01. ***p < 0.001. M-MDSCs, monocytic myeloid-derived suppressor cells.

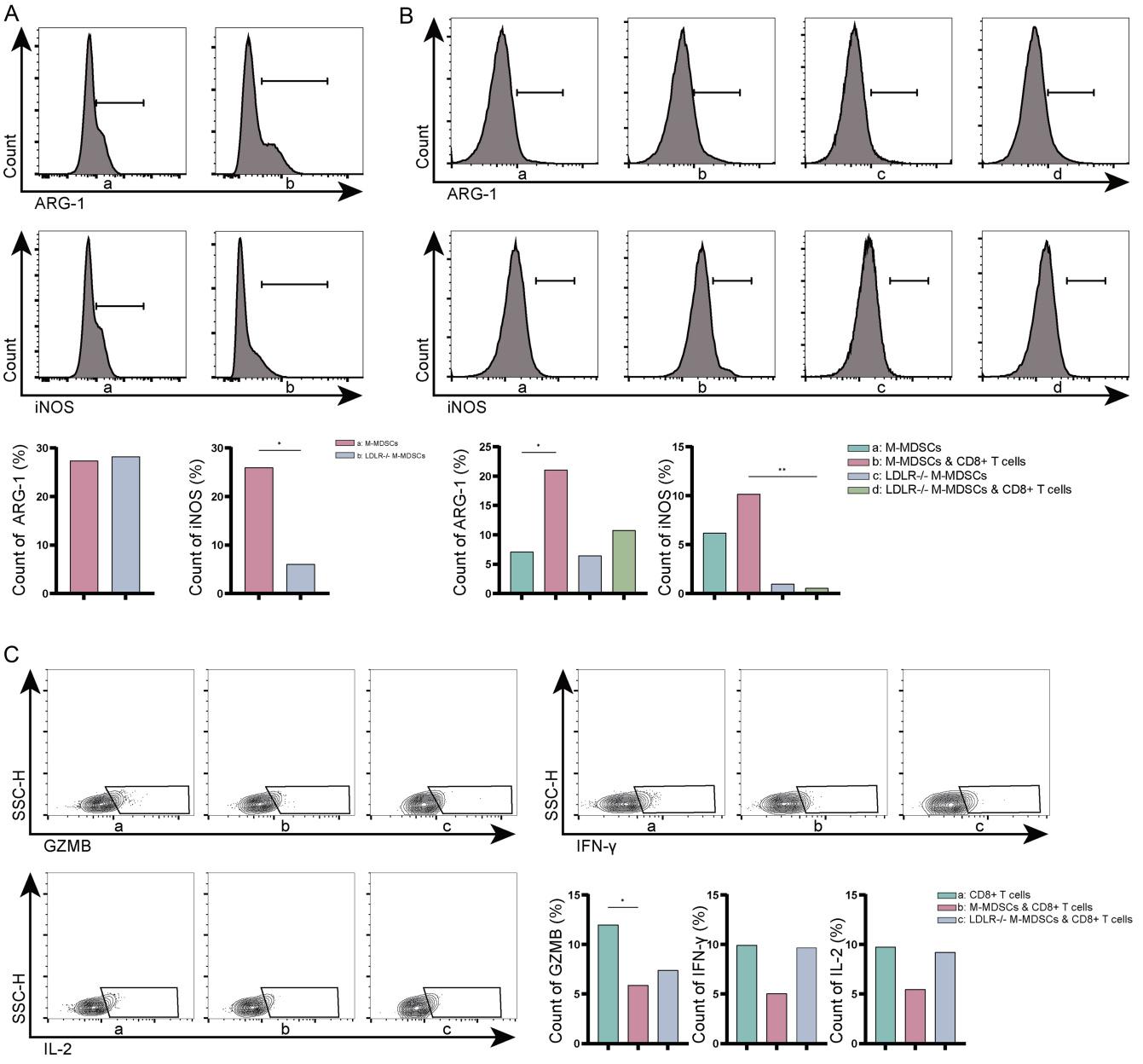

Fig. 8. Co-culture experiments of M-MDSCs and CD8$^+$ T cells. (A) Flow cytometry analysis of functional markers in M-MDSCs and LDLR−/− M-MDSCs. (B) Flow cytometry analysis of functional markers in M-MDSCs and LDLR−/− M-MDSCs co-cultured with CD8$^+$ T cells. (C) Flow cytometry analysis of functional markers in CD8$^+$ T cells co-cultured with M-MDSCs and LDLR−/− M-MDSCs. *p < 0.05. **p < 0.01. ***p < 0.001. M-MDSCs, monocytic myeloid-derived suppressor cells.

We identified three M-MDSC clusters with distinct metabolic profiles that may contribute to their immunosuppressive functions. Notably, the C1-LDLR$^+$ MDSC cluster was enriched in genes associated with lipid metabolism and protein folding, including *HSPA1A*, *HSPA1B*, and *XBP1*, suggesting a potential role in modulating endoplasmic reticulum stress. The elevated expression of *S100A8* and *S100A9*, markers linked to diminished T cell immunity and improved transplant outcomes,[54] further supports the enhanced immunosuppressive capacity. Complementary murine scRNA-seq data reveal that the C2-LDLR$^+$ MDSC shows enrichment in genes related to immune regulation (*IL1RN*, *FCGR2B*, and *TREM2*), cell adhesion and migration (*TGFBI*, *FN1*, and *SDC4*), and signal transduction (*DOK2*, *MS4A6D*, and *PHLDA1*). Additionally, dynamic variation in MDSC scores across time points exhibited a distinct temporal pattern.

During the acute phase following LT, the proportion of MDSCs increased significantly, with rejection tissues displaying markedly elevated expression of MDSC marker genes. These observations are consistent with the known functional characteristics of MDSCs in inflammatory settings, suggesting that M-MDSCs are recruited to sites of inflammation through classical monocytic trafficking pathways to mitigate tissue damage.[55] However, immunosuppressive therapies, including glucocorticoids and CNIs, have been shown to influence the mobilization and functional activity of MDSCs.[56–58] Simi-

lar trends have been reported in kidney and small intestine transplantation, where sustained M-MDSC levels contribute to Treg expansion and improved graft survival.[59–63] In parallel, liver transplant recipients experiencing rejection exhibit higher static proportions of M-MDSCs.[64] The mouse OLT models validated these dynamic patterns. Flow cytometry analyses of the liver, bone marrow, and peripheral blood in mice revealed trends in M-MDSC populations—including LDLR$^+$ M-MDSCs—that closely mirrored clinical observations. These findings provide strong evidence that M-MDSCs, particularly the LDLR$^+$ subset, play a pivotal immunosuppressive role in liver transplant rejection. Furthermore, the parallel expression of NECTIN2 and PDL1 with LDLR suggests that immune checkpoint pathways may mediate the immunosuppressive effects of these cells.

The immune system regulates appropriate responses through a balance of co-stimulatory and inhibitory signals. In acute liver transplant rejection, the activation and proliferation of CD8$^+$ T cells represent key mechanisms driving graft injury.[15,16] Consequently, promoting functional exhaustion of CD8$^+$ T cells may serve as an effective strategy to attenuate transplant rejection and preserve graft function. Functionally, exhausted T cells diverge from effector and memory T cells by exhibiting a loss of effector function and increased expression of inhibitory receptors. Spatial analysis via mIHC in mice revealed significant clustering of LDLR$^+$ M-MDSCs and TIGIT$^+$ CD8$^+$ T cells during the tolerance-prone phase (four weeks post-LT), suggesting that LDLR$^+$ M-MDSCs may contribute to the induction of CD8$^+$ T cell exhaustion. Effector T cells are typically marked by the expression of IFN-γ, GZMB, and IL-2, which distinguish them from exhausted T cells.[65,66]

MDSCs suppress T cell function primarily through the actions of ARG-1 and iNOS.[11,67] ARG-1 depletes L-arginine in the T cell microenvironment, thereby impairing T cell receptor signaling and inhibiting proliferation. Additionally, ARG-1 contributes to the differentiation of Th17 cells and Tregs.[65,68] iNOS catalyzes the production of NO in large quantities, which suppresses T cell activation and induces apoptosis.[69–71] We first assessed the expression of functional molecules in wild-type M-MDSCs and LDLR$^{-/-}$ M-MDSCs using flow cytometry. The analysis revealed a significant reduction in iNOS expression in LDLR$^{-/-}$ M-MDSCs. Co-culture experiments further showed that, upon stimulation by CD8$^+$ T cells, wild-type M-MDSCs exhibited increased expression of both ARG-1 and iNOS, whereas LDLR$^{-/-}$ M-MDSCs displayed an upregulation of ARG-1 alone. These findings suggest that wild-type M-MDSCs exert their immunosuppressive effects, at least in part, through elevated iNOS expression, and that LDLR modulates iNOS expression via an as-yet undefined regulatory pathway. Together, these results—including changes in effector molecule and inhibitory receptor expression in CD8$^+$ T cells, alongside altered functional marker expression in M-MDSCs—demonstrate a diminished immunosuppressive capacity in LDLR$^{-/-}$ M-MDSCs. This highlights the essential role of LDLR in supporting the immunosuppressive function of M-MDSCs.

Moreover, in the mouse OLT model, we concurrently detected the expression of the immune checkpoint molecules NECTIN2 and PDL1 in M-MDSCs, with expression patterns closely paralleling those of LDLR$^+$ M-MDSCs. These findings suggest that during liver transplant rejection, LDLR$^+$ M-MDSCs may mediate immunosuppressive effects through ARG-1, iNOS, and immune checkpoint pathways, with iNOS serving as a particularly distinctive and functionally relevant marker.

Changes in metabolic states significantly affect MDSC activity. In dyslipidemia, elevated CCR5 expression in M-MDSCs enhances their sensitivity to chemokines, thereby promoting their accumulation in inflammatory regions.[70,72] Variations in LDLR expression in M-MDSCs may be associated with alterations in cholesterol metabolism before and after LT. Prior to transplantation, patients with end-stage liver disease often exhibit reduced cholesterol levels due to malnutrition and diminished activity of synthetic enzymes. SREBP2, a key transcriptional regulator of LDLR, is modulated by intracellular cholesterol content, thereby influencing LDLR expression.[73] Following transplantation, nutritional support and recovery of liver function typically lead to increased cholesterol levels, potentially triggering a reactive upregulation of LDLR expression during the acute phase. Over time, LDLR levels may stabilize as the patient's clinical condition improves. Cholesterol metabolism plays a critical role in regulating the immune microenvironment, impacting both innate and adaptive immune responses.[74] In hepatocellular carcinoma, reduced LDLR expression promotes tumor progression by disrupting cholesterol homeostasis.[75] In addition to its role in cholesterol transport, LDLR functions as an immunoregulatory membrane protein essential for the activation, proliferation, and effector functions of CD8$^+$ T cells.[76] Therefore, LDLR may influence MDSC function by modulating cholesterol homeostasis within these cells.

In this study, LDLR$^+$ M-MDSCs were identified as a functionally superior immunosuppressive subset with distinct temporal and spatial dynamics following LT. These cells expanded during the acute post-transplantation phase and early rejection in mouse OLT models, declined with immune stabilization, and exhibited a close spatial and functional association with exhausted CD8$^+$ T cells within the graft. This pattern suggests that LDLR$^+$ M-MDSCs may serve as a potential non-invasive biomarker for immune status stratification, allowing dynamic assessment of rejection risk or transition toward immune tolerance beyond static histological evaluation. Clinically, sustained elevation of circulating LDLR$^+$ M-MDSCs may indicate ongoing alloimmune activation and unresolved rejection, thereby facilitating earlier optimization of individualized immunosuppressive regimens. Furthermore, LDLR$^+$ M-MDSCs represent a promising therapeutic target, as their ability to induce CD8$^+$ T cell exhaustion via ARG-1, iNOS, and immune checkpoint pathways supports strategies to selectively enhance this subset to promote graft tolerance. The association between LDLR expression, lipid metabolism, and the immunoregulatory function of M-MDSCs highlights immunometabolism as a clinically actionable axis that can be pharmacologically modulated through the LDLR pathway. Notably, PCSK9 inhibitors, which prevent LDLR degradation[77] and have been shown in oncology to enhance CD8$^+$ T cell–mediated antitumor immunity,[78] offer a particularly compelling therapeutic option. In the context of LT for hepatocellular carcinoma, PCSK9 inhibition may confer dual benefits by simultaneously augmenting antitumor immunity and enhancing M-MDSC-mediated suppression to promote graft acceptance, a hypothesis that warrants further investigation.

This study has several limitations. First, although peripheral blood flow cytometry data from clinical patients revealed trends in MDSCs, the relatively small sample size limited the depth of subsequent analyses. In addition, the functional experiments involving LDLR$^+$ M-MDSCs did not comprehensively examine metabolic differences, thereby constraining the understanding of the underlying mechanisms. Addressing these limitations in future research will be essential for achieving a more comprehensive understanding of the role of MDSCs in LT.

Conclusions

MDSCs play a pivotal role in liver transplant rejection. This study advances the understanding of MDSC-mediated immune tolerance and highlights the critical influence of LDLR expression on the immunosuppressive capacity of M-MDSCs. Further investigation is needed to elucidate the underlying immunoregulatory mechanisms and the therapeutic potential of LDLR$^+$ M-MDSCs, which may inform novel strategies to improve transplant outcomes and advance the field of transplant immunology.

Acknowledgments

The authors would like to thank Prof. Qi Ling (Zhejiang University) and Dr. Fangxue Gong (Qingdao Women and Children's Hospital) for their kind assistance, and Medjaden Inc. for the scientific editing of this manuscript.

Funding

This work was supported by the National Natural Science Foundation of China (No. 82370666), the Natural Science Foundation of Shandong Province (No. ZR2022MH292), the Science Foundation of Qingdao Science and Technology Bureau (No. 24-1-8-smjk-1-nsh), the Natural Science Foundation of Fujian Province (No. 2021J01779 and No. 2021J02041), the Joint Funds for the Innovation of Science and Technology of Fujian Province (No. 2020Y9089), and the Fujian Provincial Health Technology Project (No. 2023CXA014 and 2024CXA010).

Conflict of interest

The authors have no conflict of interest related to this publication.

Author contributions

Writing – original draft (XZ), writing – review & editing (XZ, SL, JC), conceptualization (XZ, XL, SL), formal analysis (XZ, XL), data curation (XZ, XL), visualization (XL, HC), methodology (PJ), validation (ZJ, XW, HC), resources (HL), investigation (RD), project administration (JC), funding acquisition (JC), and supervision (JC). All authors have approved the final version and publication of the manuscript.

Ethical statement

This study was performed in line with the principles of the Declaration of Helsinki (as revised in 2024). Approval was granted by the ethics committee of the Affiliated Hospital of Qingdao University (IRB: QYFYWZLL29370) and the Animal Welfare and Ethics Committee of Qingdao University (Approval No. 20221205C57C3H19220251205159). Informed consent was obtained from all individual participants included in the study. No organs/tissues were obtained from prisoners, and the organs/tissues were obtained from the Affiliated Hospital of Qingdao University. All animals received human care.

Data sharing statement

The datasets presented in this study can be accessed from online repositories. The name of the repository and accession numbers are provided below: NGDC Genome Sequence Archive (https://ngdc.cncb.ac.cn/gsa-human/); HRA002091 and HRA007802. The datasets used or analyzed during the current study are available from the corresponding author upon reasonable request.

References

[1] Azhie A, Sheth P, Hammad A, Woo M, Bhat M. Metabolic Complications in Liver Transplantation Recipients: How We Can Optimize Long-Term Survival. Liver Transpl 2021;27(10):1468–1478. doi:10.1002/lt.26219, PMID:34165872.
[2] Loupy A, Preka E, Chen X, Wang H, He J, Zhang K. Reshaping transplantation with AI, emerging technologies and xenotransplantation. Nat Med 2025;31(7):2161–2173. doi:10.1038/s41591-025-03801-9, PMID:40659768.
[3] Lucey MR, Furuya KN, Foley DP. Liver Transplantation. N Engl J Med 2023;389(20):1888–1900. doi:10.1056/NEJMra2200923, PMID:37966287.
[4] Wang P, Jiang Z, Wang C, Liu X, Li H, Xu D, *et al*. Immune Tolerance Induction Using Cell-Based Strategies in Liver Transplantation: Clinical Perspectives. Front Immunol 2020;11:1723. doi:10.3389/fimmu.2020.01723, PMID:33013824.
[5] Zhang W, Liu Z, Xu X. Navigating immune cell immunometabolism after liver transplantation. Crit Rev Oncol Hematol 2021;160:103227. doi:10.1016/j.critrevonc.2021.103227, PMID:33675906.
[6] Pan Q, Zhou A, Wang B, Xiao W, Gao Y, Liu H, *et al*. Diagnostic and predictive biomarkers of acute rejection after liver transplantation. Int J Surg 2025;111(6):3908–3919.doi:10.1097/JS9.0000000000002358,PMID:40505038.
[7] Wang R, Peng X, Yuan Y, Shi B, Liu Y, Ni H, *et al*. Dynamic immune recovery process after liver transplantation revealed by single-cell multiomics analysis. Innovation (Camb) 2024;5(3):100599. doi:10.1016/j.xinn.2024.100599, PMID:38510071.
[8] Gabrilovich DI, Nagaraj S. Myeloid-derived suppressor cells as regulators of the immune system. Nat Rev Immunol 2009;9(3):162–174. doi:10.1038/nri2506, PMID:19197294.
[9] Gabrilovich DI, Bronte V, Chen SH, Colombo MP, Ochoa A, Ostrand-Rosenberg S, *et al*. The terminology issue for myeloid-derived suppressor cells. Cancer Res 2007;67(1):425. doi:10.1158/0008-5472.CAN-06-3037, PMID:17210725.
[10] Veglia F, Sanseviero E, Gabrilovich DI. Myeloid-derived suppressor cells in the era of increasing myeloid cell diversity. Nat Rev Immunol 2021;21(8):485–498. doi:10.1038/s41577-020-00490-y, PMID:33526920.
[11] Zhang C, Wang H, Aji T, Li Z, Li Y, Ainiwaer A, *et al*. Author Correction: Targeting myeloid-derived suppressor cells promotes antiparasitic T-cell immunity and enhances the efficacy of PD-1 blockade. Nat Commun 2024;15(1):7374. doi:10.1038/s41467-024-51832-6, PMID:39191752.
[12] Zhang Z, Huang W, Hu D, Jiang J, Zhang J, Wu Z, *et al*. E-twenty-six-specific sequence variant 5 (ETV5) facilitates hepatocellular carcinoma progression and metastasis through enhancing polymorphonuclear myeloid-derived suppressor cell (PMN-MDSC)-mediated immunosuppression. Gut 2025;74(7):1137–1149. doi:10.1136/gutjnl-2024-333944, PMID:40015948.
[13] Ochando J, Conde P, Utrero-Rico A, Paz-Artal E. Tolerogenic Role of Myeloid Suppressor Cells in Organ Transplantation. Front Immunol 2019;10:374. doi:10.3389/fimmu.2019.00374, PMID:30894860.
[14] Shao L, Pan S, Zhang QP, Jamal M, Rushworth GM, Xiong J, *et al*. Emerging Role of Myeloid-derived Suppressor Cells in the Biology of Transplantation Tolerance. Transplantation 2020;104(3):467–475. doi:10.1097/TP.0000000000002996, PMID:31596739.
[15] Li X, Li S, Wu B, Xu Q, Teng D, Yang T, *et al*. Landscape of Immune Cells Heterogeneity in Liver Transplantation by Single-Cell RNA Sequencing Analysis. Front Immunol 2022;13:890019. doi:10.3389/fimmu.2022.890019, PMID:35619708.
[16] Li X, Li S, Wang Y, Zhou X, Wang F, Muhammad I, *et al*. Single cell RNA-sequencing delineates CD8(+) tissue resident memory T cells maintaining rejection in liver transplantation. Theranostics 2024;14(12):4844–4860. doi:10.7150/thno.96928, PMID:39239518.
[17] Li SP, Li XQ, Chen XJ, Zhang JM, Zhou GP, Zhou LX, *et al*. Characterization and Proteomic Analyses of Proinflammatory Cytokines in a Mouse Model of Liver Transplant Rejection. Oxid Med Cell Longev 2022;2022:5188584. doi:10.1155/2022/5188584, PMID:35993024.
[18] Hočevar S, Puddinu V, Haeni L, Petri-Fink A, Wagner J, Alvarez M, *et al*. PEGylated Gold Nanoparticles Target Age-Associated B Cells In Vivo. ACS Nano 2022;16(11):18119–18132. doi:10.1021/acsnano.2c04871, PMID:36301574.
[19] Deng S, Zhang Y, Wang H, Liang W, Xie L, Li N, *et al*. ITPRIPL1 binds CD3ε to impede T cell activation and enable tumor immune evasion. Cell 2024;187(9):2305–2323.e33. doi:10.1016/j.cell.2024.03.019, PMID:38614099.
[20] Shen DD, Pang JR, Bi YP, Zhao LF, Li YR, Zhao LJ, *et al*. LSD1 deletion decreases exosomal PD-L1 and restores T-cell response in gastric cancer. Mol Cancer 2022;21(1):75. doi:10.1186/s12943-022-01557-1, PMID:35296335.
[21] An R, Yang H, Tang C, Li Q, Huang Q, Wang H, *et al*. A protein vaccine of RBD integrated with immune evasion mutation shows broad protection against SARS-CoV-2. Signal Transduct Target Ther 2024;9(1):301. doi:10.1038/s41392-024-02007-8, PMID:39500906.
[22] Wang B, Wang L, Shang R, Xie L. MDSC suppresses T cell antitumor immunity in CAC via GPNMB in a MyD88-dependent manner. Cancer Med

2024;13(1):e6887. doi:10.1002/cam4.6887, PMID:38140790.
[23] Hao Y, Hao S, Andersen-Nissen E, Mauck WM 3rd, Zheng S, Butler A, *et al*. Integrated analysis of multimodal single-cell data. Cell 2021;184(13):3573–3587.e29. doi:10.1016/j.cell.2021.04.048, PMID:34062119.
[24] Jiang P, Luo L, Li X, Cai K, Chen S, Teng D, *et al*. PTX3 exacerbates hepatocyte pyroptosis in hepatic ischemia-reperfusion injury by promoting macrophage M1 polarization. Int Immunopharmacol 2024;143(Pt 3):113604. doi:10.1016/j.intimp.2024.113604, PMID:39549552.
[25] Shi S, Zhu C, Shi S, Li X, Muhammad I, Xu Q, *et al*. Human spindle-shaped urine-derived stem cell exosomes alleviate severe fatty liver ischemia-reperfusion injury by inhibiting ferroptosis via GPX4. Stem Cell Res Ther 2025;16(1):81. doi:10.1186/s13287-025-04202-y, PMID:39985001.
[26] Li X, Li R, Miao X, Zhou X, Wu B, Cao J, *et al*. Integrated Single Cell Analysis Reveals An Atlas of Tumor Associated Macrophages in Hepatocellular Carcinoma. Inflammation 2024;47(6):2077–2093. doi:10.1007/s10753-024-02026-1, PMID:38668836.
[27] Hu C, Li T, Xu Y, Zhang X, Li F, Bai J, *et al*. CellMarker 2.0: an updated database of manually curated cell markers in human/mouse and web tools based on scRNA-seq data. Nucleic Acids Res 2023;51(D1):D870–D876. doi:10.1093/nar/gkac947, PMID:36300619.
[28] Wu T, Hu E, Xu S, Chen M, Guo P, Dai Z, *et al*. clusterProfiler 4.0: A universal enrichment tool for interpreting omics data. Innovation (Camb) 2021;2(3):100141. doi:10.1016/j.xinn.2021.100141, PMID:34557778.
[29] Alshetaiwi H, Pervolarakis N, McIntyre LL, Ma D, Nguyen Q, Rath JA, *et al*. Defining the emergence of myeloid-derived suppressor cells in breast cancer using single-cell transcriptomics. Sci Immunol 2020;5(44):eaay6017. doi:10.1126/sciimmunol.aay6017, PMID:32086381.
[30] Jin S, Guerrero-Juarez CF, Zhang L, Chang I, Ramos R, Kuan CH, *et al*. Inference and analysis of cell-cell communication using CellChat. Nat Commun 2021;12(1):1088. doi:10.1038/s41467-021-21246-9, PMID:33597522.
[31] Madill-Thomsen K, Abouljoud M, Bhati C, Ciszek M, Durlik M, Feng S, *et al*. The molecular diagnosis of rejection in liver transplant biopsies: First results of the INTERLIVER study. Am J Transplant 2020;20(8):2156–2172. doi:10.1111/ajt.15828, PMID:32090446.
[32] Qiu J, Chen L, Zhang L, Xu F, Zhang C, Ren G, *et al*. Xie Zhuo Tiao Zhi formula modulates intestinal microbiota and liver purine metabolism to suppress hepatic steatosis and pyroptosis in NAFLD therapy. Phytomedicine 2023;121:155111. doi:10.1016/j.phymed.2023.155111, PMID:37804819.
[33] Xue R, Jiang L, Zhang QR, Wang QJ, Yang RX, Ren TY, *et al*. Arctigenin Prevents Metabolic Dysfunction-associated Steatohepatitis by Inhibiting NLRP3/GSDMD-N Axis in Macrophages. J Clin Transl Hepatol 2025;13(10):809–824. doi:10.14218/JCTH.2025.00141, PMID:41089708.
[34] Erber R, Spoerl S, Mamilos A, Krupar R, Hartmann A, Ruebner M, *et al*. Impact of Spatially Heterogeneous Trop-2 Expression on Prognosis in Oral Squamous Cell Carcinoma. Int J Mol Sci 2021;23(1):87. doi:10.3390/ijms23010087, PMID:35008509.
[35] MacParland SA, Tsoi KM, Ouyang B, Ma XZ, Manuel J, Fawaz A, *et al*. Phenotype Determines Nanoparticle Uptake by Human Macrophages from Liver and Blood. ACS Nano 2017;11(3):2428–2443. doi:10.1021/acsnano.6b06245, PMID:28040885.
[36] Mei Y, Zhu Y, Yong KSM, Hanafi ZB, Gong H, Liu Y, *et al*. IL-37 dampens immunosuppressive functions of MDSCs via metabolic reprogramming in the tumor microenvironment. Cell Rep 2024;43(3):113835. doi:10.1016/j.celrep.2024.113835, PMID:38412100.
[37] Jia X, Xi J, Tian B, Zhang Y, Wang Z, Wang F, *et al*. The Tautomerase Activity of Tumor Exosomal MIF Promotes Pancreatic Cancer Progression by Modulating MDSC Differentiation. Cancer Immunol Res 2024;12(1):72–90. doi:10.1158/2326-6066.CIR-23-0205, PMID:37956411.
[38] Liu A, Gammon ST, Pisaneschi F, Boda A, Ager CR, Piwnica-Worms D, *et al*. Hypoxia-activated prodrug and antiangiogenic therapies cooperatively treat pancreatic cancer but elicit immunosuppressive G-MDSC infiltration. JCI Insight 2024;9(1):e169150. doi:10.1172/jci.insight.169150, PMID:37988164.
[39] Huang H, Chen R, Lin Y, Jiang J, Feng S, Zhang X, *et al*. Decoding Single-cell Landscape and Intercellular Crosstalk in the Transplanted Liver. Transplantation 2023;107(4):890–902. doi:10.1097/TP.0000000000004365, PMID:36413145.
[40] Zhai J, Chen H, Wong CC, Peng Y, Gou H, Zhang J, *et al*. ALKBH5 Drives Immune Suppression Via Targeting AXIN2 to Promote Colorectal Cancer and Is a Target for Boosting Immunotherapy. Gastroenterology 2023;165(2):445–462. doi:10.1053/j.gastro.2023.04.032, PMID:37169182.
[41] Li S, Zhang J, Wei W, Zhang Z, Huang W, Xia L. The important role of myeloid-derived suppressor cells: From hepatitis to liver cancer. Biochim Biophys Acta Rev Cancer 2025;1880(3):189329. doi:10.1016/j.bbcan.2025.189329, PMID:40262654.
[42] Liu Y, Ren Y, Luo R, Li X, Xie L, Kang H, *et al*. Tacrolimus prolongs corneal allograft survival and prevents dendritic cell infiltration in a myeloid-derived suppressor cell-dependent manner. Am J Transplant 2025;25(9):1870–1883. doi:10.1016/j.ajt.2025.05.018, PMID:40398562.
[43] Halaby MJ, Hezaveh K, Lamorte S, Ciudad MT, Kloetgen A, MacLeod BL, *et al*. GCN2 drives macrophage and MDSC function and immunosuppression in the tumor microenvironment. Sci Immunol 2019;4(42):eaax8189. doi:10.1126/sciimmunol.aax8189, PMID:31836669.
[44] Liu JL, Xu X, Rixiati Y, Wang CY, Ni HL, Chen WS, *et al*. Dysfunctional circadian clock accelerates cancer metastasis by intestinal microbiota triggering accumulation of myeloid-derived suppressor cells. Cell Metab 2024;36(6):1320–1334.e9. doi:10.1016/j.cmet.2024.04.019, PMID:38838643.
[45] Xie Z, Ikegami T, Ago Y, Okada N, Tachibana M. Valproic acid attenuates CCR2-dependent tumor infiltration of monocytic myeloid-derived suppressor cells, limiting tumor progression. Oncoimmunology 2020;9(1):1734268. doi:10.1080/2162402X.2020.1734268, PMID:32158627.
[46] Liu H, Ling CC, Yeung WHO, Pang L, Liu J, Zhou J, *et al*. Monocytic MDSC mobilization promotes tumor recurrence after liver transplantation via CXCL10/TLR4/MMP14 signaling. Cell Death Dis 2021;12(5):489. doi:10.1038/s41419-021-03788-4, PMID:33990548.
[47] Horn CM, Arumugam P, Van Roy Z, Heim CE, Fallet RW, Bertrand BP, *et al*. Granulocytic myeloid-derived suppressor cell activity during biofilm infection is regulated by a glycolysis/HIF1a axis. J Clin Invest 2024;134(8):e174051. doi:10.1172/JCI174051, PMID:38421730.
[48] Ohl K, Tenbrock K. Reactive Oxygen Species as Regulators of MDSC-Mediated Immune Suppression. Front Immunol 2018;9:2499. doi:10.3389/fimmu.2018.02499, PMID:30425715.
[49] Sprouse ML, Welte T, Boral D, Liu HN, Yin W, Vishnoi M, *et al*. PMN-MDSCs Enhance CTC Metastatic Properties through Reciprocal Interactions via ROS/Notch/Nodal Signaling. Int J Mol Sci 2019;20(8):1916. doi:10.3390/ijms20081916, PMID:31003475.
[50] Yan L, Liang M, Yang T, Ji J, Jose Kumar Sreena GS, Hou X, *et al*. The Immunoregulatory Role of Myeloid-Derived Suppressor Cells in the Pathogenesis of Rheumatoid Arthritis. Front Immunol 2020;11:568362. doi:10.3389/fimmu.2020.568362, PMID:33042149.
[51] Cassetta L, Bruderek K, Skrzeczynska-Moncznik J, Osiecka O, Hu X, Rundgren IM, *et al*. Differential expansion of circulating human MDSC subsets in patients with cancer, infection and inflammation. J Immunother Cancer 2020;8(2):e001223. doi:10.1136/jitc-2020-001223, PMID:32907925.
[52] Tan Z, Chiu MS, Yue M, Kwok HY, Tse MH, Wen Y, *et al*. Enhancing the efficacy of vaccinia-based oncolytic virotherapy by inhibiting CXCR2-mediated MDSC trafficking. J Leukoc Biol 2024;115(4):633–646. doi:10.1093/jleuko/qiad150, PMID:38066571.
[53] Sun X, Hou J, Ni T, Xu Z, Yan W, Kong L, *et al*. MCC950 attenuates plasma cell mastitis in an MDSC-dependent manner. Int Immunopharmacol 2024;131:111803. doi:10.1016/j.intimp.2024.111803, PMID:38460298.
[54] Rekers NV, Bajema IM, Mallat MJ, Petersen B, Anholts JD, Swings GM, *et al*. Beneficial Immune Effects of Myeloid-Related Proteins in Kidney Transplant Rejection. Am J Transplant 2016;16(5):1441–1455. doi:10.1111/ajt.13634, PMID:26607974.
[55] Leroy V, Manual Kollareth DJ, Tu Z, Valisno JAC, Woolet-Stockton M, Saha B, *et al*. MerTK-dependent efferocytosis by monocytic-MDSCs mediates resolution of post-lung transplant injury. bioRxiv 2024. doi:10.1101/2024.01.18.576261, PMID:38328174.
[56] Iglesias-Escudero M, Segundo DS, Merino-Fernandez D, Mora-Cuesta VM, Lamadrid P, Alonso-Peña M, *et al*. Myeloid-Derived Suppressor Cells Are Increased in Lung Transplant Recipients and Regulated by Immunosuppressive Therapy. Front Immunol 2021;12:788851. doi:10.3389/fimmu.2021.788851, PMID:35185863.
[57] Lee HJ, Park SY, Jeong HJ, Kim HJ, Kim MK, Oh JY. Glucocorticoids induce corneal allograft tolerance through expansion of monocytic myeloid-derived suppressor cells. Am J Transplant 2018;18(12):3029–3037. doi:10.1111/ajt.15026, PMID:30019411.
[58] Zhao Y, Shen XF, Cao K, Ding J, Kang X, Guan WX, *et al*. Dexamethasone-Induced Myeloid-Derived Suppressor Cells Prolong Allo Cardiac Graft Survival through iNOS- and Glucocorticoid Receptor-Dependent Mechanism. Front Immunol 2018;9:282. doi:10.3389/fimmu.2018.00282, PMID:29497426.
[59] Luan Y, Mosheir E, Menon MC, Wilson D, Woytovich C, Ochando J, *et al*. Monocytic myeloid-derived suppressor cells accumulate in renal transplant patients and mediate CD4(+) Foxp3(+) Treg expansion. Am J Transplant 2013;13(12):3123–3131. doi:10.1111/ajt.12461, PMID:24103111.
[60] Meng F, Chen S, Guo X, Chen Z, Huang X, Lai Y, *et al*. Clinical significance of myeloid-derived suppressor cells in human renal transplantation with acute T cell-mediated rejection. Inflammation 2014;37(5):1799–1805. doi:10.1007/s10753-014-9910-5, PMID:24788988.
[61] Iglesias-Escudero M, Sansegundo-Arribas D, Riquelme P, Merino-Fernández D, Guiral-Foz S, Pérez C, *et al*. Myeloid-Derived Suppressor Cells in Kidney Transplant Recipients and the Effect of Maintenance Immunotherapy. Front Immunol 2020;11:643. doi:10.3389/fimmu.2020.00643, PMID:32425928.
[62] Utrero-Rico A, Laguna-Goya R, Cano-Romero F, Chivite-Lacaba M, Gonzalez-Cuadrado C, Rodríguez-Sánchez E, *et al*. Early Posttransplant Mobilization of Monocytic Myeloid-derived Suppressor Cell Correlates With Increase in Soluble Immunosuppressive Factors and Predicts Cancer in Kidney Recipients. Transplantation 2020;104(12):2599–2608. doi:10.1097/TP.0000000000003179, PMID:32068661.
[63] Okano S, Abu-Elmagd K, Kish DD, Keslar K, Baldwin WM 3rd, Fairchild RL, *et al*. Myeloid-derived suppressor cells increase and inhibit donor-reactive T cell responses to graft intestinal epithelium in intestinal transplant patients. Am J Transplant 2018;18(10):2544–2558. doi:10.1111/ajt.14718, PMID:29509288.
[64] Zhou LX, Jiang YZ, Li XQ, Zhang JM, Li SP, Wei L, *et al*. Myeloid-derived suppressor cells-induced exhaustion of CD8 + T-cell participates in rejection after liver transplantation. Cell Death Dis 2024;15(7):507. doi:10.1038/s41419-024-06834-z, PMID:39013845.
[65] Ajith A, Mamouni K, Horuzsko DD, Musa A, Dzutsev AK, Fang JR, *et al*. Targeting TREM1 augments antitumor T cell immunity by inhibiting myeloid-derived suppressor cells and restraining anti-PD-1 resistance. J Clin Invest 2023;133(21):e167951. doi:10.1172/JCI167951, PMID:37651197.
[66] Jensen KP, Hongo DA, Ji X, Zheng P, Pawar R, Wu TH, *et al*. Development of immunosuppressive myeloid cells to induce tolerance in solid organ and hematopoietic cell transplant recipients. Blood Adv 2021;5(17):3290–3302. doi:10.1182/bloodadvances.2020003669, PMID:34432869.
[67] Zhang W, Li J, Qi G, Tu G, Yang C, Xu M. Myeloid-derived suppressor cells in transplantation: the dawn of cell therapy. J Transl Med 2018;16(1):19. doi:10.1186/s12967-018-1395-9, PMID:29378596.

[68] Pang B, Zhen Y, Hu C, Ma Z, Lin S, Yi H. Myeloid-derived suppressor cells shift Th17/Treg ratio and promote systemic lupus erythematosus progression through arginase-1/miR-322-5p/TGF-β pathway. Clin Sci (Lond) 2020;134(16):2209–2222. doi:10.1042/CS20200799, PMID:32808653.
[69] Mazzoni A, Bronte V, Visintin A, Spitzer JH, Apolloni E, Serafini P, *et al*. Myeloid suppressor lines inhibit T cell responses by an NO-dependent mechanism. J Immunol 2002;168(2):689–695. doi:10.4049/jimmunol.168.2.689, PMID:11777962.
[70] Fraternale A, Green KA, Schiavano GF, Bruschi M, Retini M, Magnani M, *et al*. Inhibition of myeloid-derived suppressor cell (MDSC) activity by redox-modulating agents restores T and B cell proliferative responses in murine AIDS. Int Immunopharmacol 2023;124(Pt A):110882. doi:10.1016/j.intimp.2023.110882, PMID:37659111.
[71] Arakawa Y, Qin J, Chou HS, Bhatt S, Wang L, Stuehr D, *et al*. Cotransplantation with myeloid-derived suppressor cells protects cell transplants: a crucial role of inducible nitric oxide synthase. Transplantation 2014;97(7):740–747. doi:10.1097/01.TP.0000442504.23885.f7, PMID:24642686.
[72] Chen J, Liu X, Zou Y, Gong J, Ge Z, Lin X, *et al*. A high-fat diet promotes cancer progression by inducing gut microbiota-mediated leucine production and PMN-MDSC differentiation. Proc Natl Acad Sci U S A 2024;121(20):e2306776121. doi:10.1073/pnas.2306776121, PMID:38709933.
[73] Madison BB. Srebp2: A master regulator of sterol and fatty acid synthesis. J Lipid Res 2016;57(3):333–335. doi:10.1194/jlr.C066712, PMID:26798145.
[74] Aguilar-Ballester M, Herrero-Cervera A, Vinué Á, Martínez-Hervás S, González-Navarro H. Impact of Cholesterol Metabolism in Immune Cell Function and Atherosclerosis. Nutrients 2020;12(7):2021. doi:10.3390/nu12072021, PMID:32645995.
[75] Chen Z, Chen L, Sun B, Liu D, He Y, Qi L, *et al*. LDLR inhibition promotes hepatocellular carcinoma proliferation and metastasis by elevating intracellular cholesterol synthesis through the MEK/ERK signaling pathway. Mol Metab 2021;51:101230. doi:10.1016/j.molmet.2021.101230, PMID:33823318.
[76] Yuan J, Cai T, Zheng X, Ren Y, Qi J, Lu X, *et al*. Potentiating CD8(+) T cell antitumor activity by inhibiting PCSK9 to promote LDLR-mediated TCR recycling and signaling. Protein Cell 2021;12(4):240–260. doi:10.1007/s13238-021-00821-2, PMID:33606190.
[77] Guan Y, Liu X, Yang Z, Zhu X, Liu M, Du M, *et al*. PCSK9 Promotes LDLR Degradation by Preventing SNX17-Mediated LDLR Recycling. Circulation 2025;151(21):1512–1526. doi:10.1161/CIRCULATIONAHA.124.072336, PMID:40071387.
[78] Liu X, Bao X, Hu M, Chang H, Jiao M, Cheng J, *et al*. Inhibition of PCSK9 potentiates immune checkpoint therapy for cancer. Nature 2020;588(7839):693–698. doi:10.1038/s41586-020-2911-7, PMID:33177715.